



Topographical and morphological aspects of spray coated organic photovoltaics

Claudia N. Hoth^{a,b,*}, Roland Steim^{a,c}, Pavel Schilinsky^a, Stelios A. Choulis^d, Sandro F. Tedde^e, Oliver Hayden^e, Christoph J. Brabec^{a,*}

^a Konarka Technologies GmbH, Landgrabenstr. 94, D-90443 Nürnberg, Germany

^b Department of Energy and Semiconductor Research, University of Oldenburg, D-26129 Oldenburg, Germany

^c Light Technology Institute, University of Karlsruhe (TH), D-76131 Karlsruhe, Germany

^d Department of Mechanical Engineering and Materials Science and Engineering, Cyprus University of Technology, 3603 Limassol, Cyprus

^e Siemens AG, Corporate Technology, CT MM1, Günther-Scharowsky-Str. 1, D-91058 Erlangen, Germany

ARTICLE INFO

Article history:

Received 2 December 2008

Received in revised form 13 February 2009

Accepted 14 February 2009

Available online 23 February 2009

PACS:

81.15.Rs

72.40

84.60.Jt

82.35.Cd

72.80.Le

72.80.Rj

Keywords:

Spray coating

Photovoltaics

Solar cells

Polymers

Fullerenes

P3HT

ABSTRACT

Herein we discuss the topographical and nanomorphological aspects of spray deposited organic photovoltaics. We show that the solvent properties have a massive impact on the topography, but less on the nanomorphology formation of composites based on the electron donor poly(3-hexylthiophene) (P3HT) and the electron acceptor [6,6]-phenyl C61 butyric acid methyl ester (PCBM). An adapted solvent mixture consisting of ortho-dichlorobenzene (oDCB) and 1,3,5-trimethylbenzene (mesitylene) allows us to demonstrate spray coated organic photovoltaic devices with 3.1% power conversion efficiency (PCE). Moreover, we show that spray coating is a feasible technology to deposit all solution processable layers of organic solar cells, including the hole transporting layer poly(3,4-ethylene dioxythiophene) doped with polystyrene sulphonic acid (PEDOT:PSS) as well and demonstrate fully spray coated devices with 2.7% PCE.

© 2009 Elsevier B.V. All rights reserved.

Organic photovoltaics (OPVs) are of increasing interest as new materials for future light-activated energy sources. OPVs have the virtue of being lightweight and flexible and could open up many new applications due to their easy processing offering the potential for low fabrication cost [1]. A variety of approaches have been used to deposit or-

ganic semiconductors based on the nature of those materials. The commonly applied technique is the solution-processed deposition, such as spin coating, doctor blading [2] or printing, which are evaluated as one of the future key technologies opening up completely new applications and markets for photovoltaics [1]. Printing technologies such as screen printing [3], gravure, offset, micro-contact and inkjet printing [4] are attractive candidates to utilize a low-cost OPV roll to roll production.

At present, bulk heterojunction (BHJ) structures based on blends of polymer donor and a highly soluble fullerene

* Corresponding authors. Address: Konarka Technologies GmbH, Landgrabenstr. 94, D-90443 Nürnberg, Germany (C.N. Hoth).

E-mail addresses: choth@konarka.com (C.N. Hoth), cbrabec@konarka.com (C.J. Brabec).

derivative as acceptor have been the material system with the highest reported power conversion efficiencies (PCE) [5] and the demonstration of solar cells with 5% PCE under calibrated AM 1.5 conditions have been regarded as an important milestone to prove the technology's potential [6]. Among other technologies, spray coating [7] was recently reported as an elegant coating technique for the fabrication of BHJ devices. Recently, Vak et al. showed that spray coating the active layer from chlorobenzene solutions gives highly efficient devices [8]. Furthermore, Green et al. presented spray deposited poly(3-hexylthiophene) (P3HT): [6,6]-phenyl C61 butyric acid methyl ester (PCBM) films from a variety of common organic solvents with different boiling points [9].

In this communication, we investigate spray coating as a production technique for depositing the active layer in organic BHJ solar cells. We specifically investigate the film formation, surface topography and the morphology of spray coated mono- and bilayers based on pristine solvents compared to mono- and bilayers based on multiple solvent systems. Furthermore, we studied the impact of the ink formulation and specifically the solvent properties such as vapor pressure, boiling point, viscosity and surface tension on the topography, nanomorphology

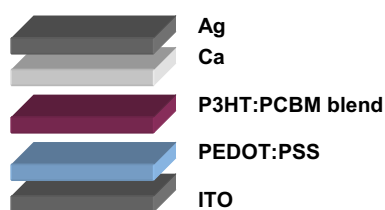


Fig. 1. Device architecture of a solar cell ITO/PEDOT:PSS/P3HT:PCBM blend/Ca/Ag under study.

Table 1
Solvent properties.

Solvent	Vapor pressure at 20 °C (mm Hg)	Boiling point (°C)	Surface tension (dynes cm ⁻¹)	Viscosity at 25 °C (mPa)
Chlorobenzene	11.70	132	33.0	0.76
ortho-Dichlorobenzene	1.20	180	37.0	1.32
Mesitylene	1.86	165	28.8	1.04

Table 2
Measured values of ink properties with appropriate random errors, thickness of spray coated active layer and rms roughness.

Ink formulation	Surface tension (dynes cm ⁻¹)	Contact angle on PEDOT:PSS (°)	Kinematic viscosity (m ² s ⁻¹)	Active layer thickness mono/bi (nm)	RMS roughness mono/bi (nm)
P3HT:PCBM in chlorobenzene (IF1)	29.5 ± 0.1	9.7 ± 0.2	1.8 ± 0.02	250/400	67.9/46.0
P3HT:PCBM in oDCB/mesitylene (IF2)	28.0 ± 0.3	7.7 ± 0.2	2.4 ± 0.2	250/400	24.1/51.7

and device performance of spray coated photoactive P3HT:PCBM films. In detail, we show that a mixture of high and low boiling solvent, in our case 68% ortho-dichlorobenzene (oDCB) and 32% 1,3,5-trimethylbenzene (mesitylene) allows to produce spray coated organic solar cells with AM 1.5 calibrated PCE of over 3.1%. Interestingly, the large surface roughness of the films does not seem to impact the device performance. Moreover, we show that spray coating is a feasible technology to deposit all solution processable layers of organic solar cells, including poly(3,4-ethylene dioxythiophene) doped with polystyrene sulphonic acid (PEDOT:PSS) as well and demonstrate fully spray coated cells with a PCE of 2.7%. The device performance of spray coated films is demonstrated based on the common device configuration glass/ITO/doctor bladed or spray coated PEDOT:PSS/spray coated active layer/Ca/Ag, depicted in Fig. 1.

In the spray coating technique, organic thin films are generated stepwise. Single droplets are deposited by the transfer gas pressure with a high velocity onto the substrate. Spray coated films are formed via droplets, drying immediately when hitting the surface of the substrate. This is very different to most conventional printing technologies such as inkjet printing [4], where the film formation is based on the spreading of droplets and combining with adjacent droplets, forming a liquid bulk that dries during vaporization of the organic solvents. To achieve rapid drying, the semiconductor ink must fulfill certain requirements, which are primarily defined by the solvent properties, such as boiling point, vapor pressure, viscosity and surface tension, as presented in Table 1. In this study, the ink is processed at ambient conditions and is not heated during the spray deposition. To be compatible with the nozzle of the airbrush, the viscosity needs to be rather low at room temperature. High viscous inks require higher temperatures to decrease the viscosity and adapt the fluid properties on the airbrush setup. If the nozzle-to-substrate distance is constant, inks with too low drying rates the liquid droplets are immediately pushed sideways by the pressure gas of the airbrush, resulting in non-uniform wetting. On the other hand, organic solvents with too high evaporation rates, at a certain nozzle-to-substrate distance the spray deposited droplets may be dry prior to reaching the substrate surface and a film deposition is inhibited. According to this, we studied two ink formulations differing in the drying behaviour. The first ink formulation is based on pristine chlorobenzene (IF1) and features a low boiling point and high vapor pressure resulting in rapid drying. The low surface tension for the blended semiconductor solutions guarantees decent wettability, which is also indicated by the small contact angle, represented in

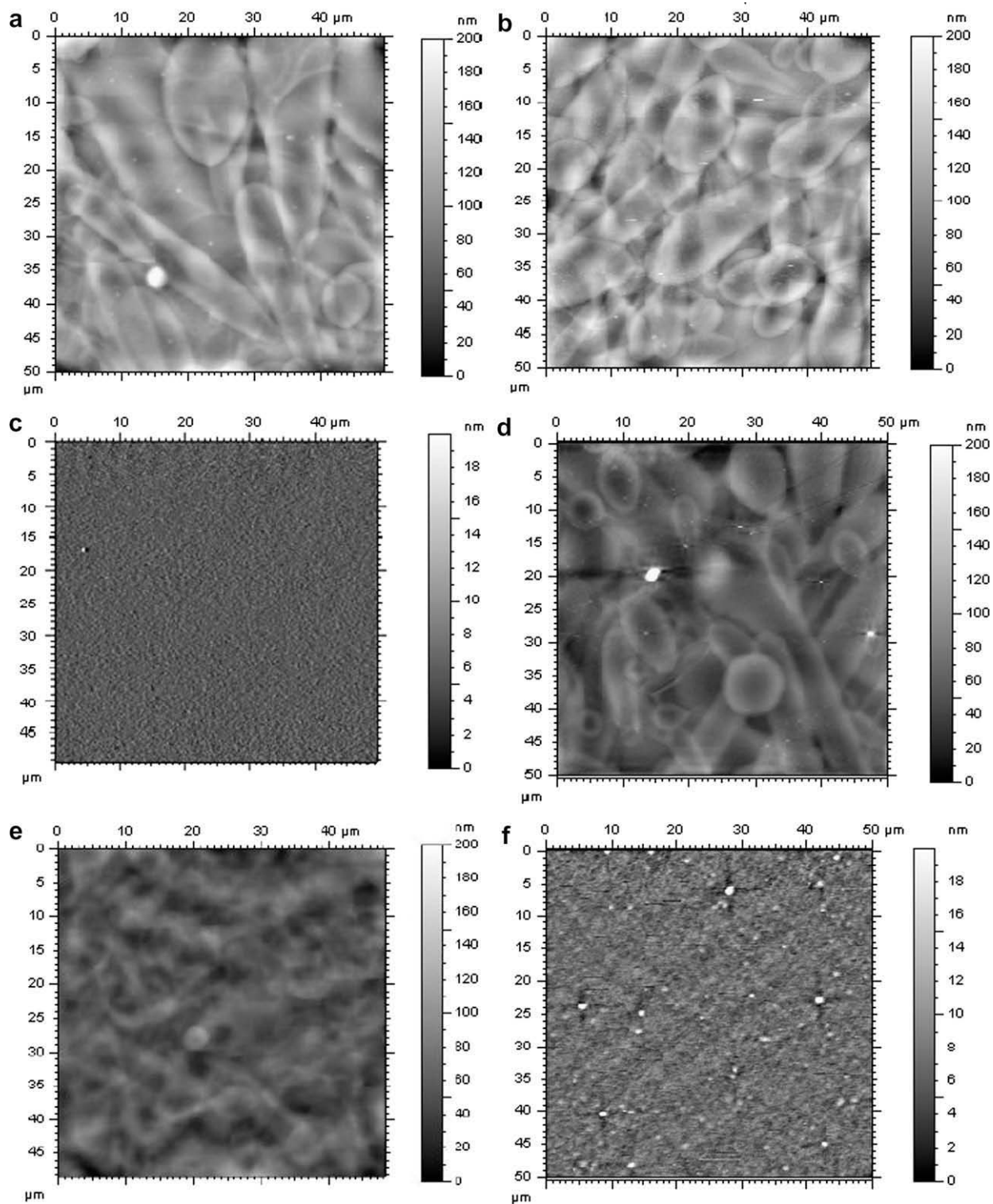


Fig. 2. AFM images representing the surface topographies of the devices under study. (a) Chlorobenzene (IF1), spray coated monolayer. (b) Chlorobenzene (IF1), spray coated bilayer. (c) Chlorobenzene (IF1), doctor bladed reference, rms 3.3 nm. (d) oDCB/mesitylene (IF2), spray coated monolayer. (e) oDCB/mesitylene (IF2), spray coated bilayer. (f) oDCB/mesitylene (IF2), doctor bladed reference, rms 4.1 nm.

Table 2. The second ink formulation is based on 68% oDCB and 32% mesitylene organic solvents (IF2) showing higher

boiling points and lower vapor pressures for a slow drying. The surface tension of the blend solution and the low

contact angle again guarantee good wettability. More details on the development of ink formulation **IF2** can be found elsewhere [4].

The atomic force microscope (AFM) images of the mono- and bilayer spray coated P3HT:PCBM films on doctor bladed PEDOT:PSS substrates are presented in Fig. 2. Due to the high surface roughness and to better reveal the film topography, the height scale is chosen to be 200 nm for all spray deposited layers. For both ink formulations, the spray coated films demonstrate a significantly larger grain size and higher roughness compared to doctor bladed layers. Single dried droplets are identified and indicate a stepwise film formation. Considering **IF1** spray deposited active layers (Fig. 2a and b), the monolayer (Fig. 2a) exhibits an rms roughness of 67.9 nm, whereas the rms roughness of the bilayer sprayed film (Fig. 2b) could be reduced to 46.0 nm due to smaller droplet sizes while depositing the film in two steps (bilayer). In this study, the thickness of mono- and bilayers for both ink formulations was adjusted to 250 and 400 nm, respectively. The overall film thickness can be varied by the spraying time interval, the droplet size and the flow rate. To obtain a 400 nm thickness for bilayer sprayed films, the flow volume per time was slightly reduced compared to monolayers, resulting in smaller droplets. Otherwise, by using the same spraying parameter as for monolayers, the film thickness would be doubled. With this spray coating setup it was not possible to obtain equal film thicknesses of 250 nm for both, mono- and bilayers without altering the spraying parameters nozzle distance and ink flow rate as well as solution concentrations significantly. This modification would lead to entirely different processing conditions for mono- and bilayers, which prevent a fair comparison between **IF1** and **IF2**. Therefore, we set the film thickness to 250 nm for monolayers and 400 nm for bilayers. We achieved the same film thickness for **IF1** and **IF2**, measured by both AFM, as well as optical absorption measurement (Fig. S3). The lower surface roughness for **IF1** bilayers is explained by the smaller droplets. Spraying the second layer, the droplets fill the gaps produced by the first sprayed layer and thus, the overall surface roughness is reduced. The doctor bladed reference film is shown in Fig. 2c and provides a completely different topography with very smooth layer and little grain sizes resulting in an rms roughness of only 3.3 nm.

The spray deposited monolayer based on **IF2** (Fig. 2d) demonstrates a considerably lower rms roughness of 24.1 nm compared to the monolayer from **IF1**. Using identical nozzle-to-substrate distances for both ink formulations but decreased ink flow rates for **IF2** over **IF1**, the dried droplets based on **IF2** show a smaller diameter and a more circular shape. The lower rms roughness can be related to the improved wetting behaviour of **IF2** due to the low surface tension of the component mesitylene which results in an overall decreased surface tension of the P3HT:PCBM-**IF2** and a lower contact angle on doctor bladed PEDOT:PSS. Regarding the **IF2** spray deposited bilayer (Fig. 2e) with its rms roughness of 51.7 nm, the surface topography indicates significant differences in the film formation compared to **IF1** bilayers (Fig. 2b). While the AFM image of the **IF1** bilayer clearly exhibits individu-

ally dried droplets from two sequential steps, the film formation of the **IF2** bilayer (Fig. 2e) is dominated by the film forming dynamics, where the second layer partially redissolves the first layer. This difference in the surface topography between the **IF1** bilayer and **IF2** bilayer is attributed to the differences in boiling points and, more important, to distinct vapor pressures by almost a factor 10. According to the higher vapor pressure and thus, faster drying condition, the spray deposition of a second **IF1** layer will not influence/reorder and redissolve the first **IF1** layer as much as the second **IF2** layer, since all deposited droplets are dried at their impact. This is also consistent with Fig. 2b showing clear dried droplets and a sequential film formation of the **IF1** bilayer. While spraying a second **IF2** layer on top of a first layer, leads to a reordering and mixing between the two layers due to a lower drying rate of **IF2** and therefore, the droplets contain higher solvent residual at their impact. This reorganization does affect the film quality and the morphology which is in good accordance with the AFM image in Fig. 2e showing a more blended structure of the two successive deposited layers. If the droplets are not dry at all or too wet at their impact, spray coating as a deposition method is not capable, since the droplets would not adhere to the substrate, but rather pushed sideways due to the transfer gas pressure. The doctor bladed reference film based on **IF2** is demonstrated in Fig. 2f with observably smaller grain sizes and rms roughness is calculated to be 4.1 nm. The AFM analysis of the spray coated films indicates significant distinctions in the surface topography compared to doctor bladed films. In the next paragraph, we will discuss whether differences in film topography can be related to differences in nanomorphology and device performance.

The nanomorphology of mono- or bilayer spray coated films was investigated by analyzing the device performance of organic solar cells. The cells were fabricated in an identical manner using either **IF1** or **IF2** as organic solvents for the spray deposition of the P3HT:PCBM active layer on doctor bladed PEDOT:PSS (see Section 1). A statistical analysis of the solar cell device parameters under AM 1.5 illumination can be found in the supplementary information (Fig. S1). The **IF2** monolayer (Fig. 2d) is formed by depositing smaller droplets yielding a more uniform film with decreased rms roughness (Table 2) and a lower pinhole density. Correspondingly, the shunt is reduced while the fill factor (*FF*) and open circuit voltage (*V_{oc}*) increase, as also indicated by the representative current–voltage (*J–V*) behaviour under illumination shown in Fig. 3b. A better molecular distribution of PCBM within the P3HT domains and the improved intermixing of the first and second spray deposited layer for the **IF2** bilayer are indicated by a reduced reverse bias dependence of the photocurrent and results in significant better charge transport properties (Fig. 3).

For a detailed investigation of the morphology, the current–voltage behaviour of representative solar cell devices is analyzed [10].

$$J = J_0 \left(e^{\frac{-q(V - JR_S)}{nkT}} - 1 \right) + \frac{V - JR_S}{R_p} + J_{light} \quad (1)$$

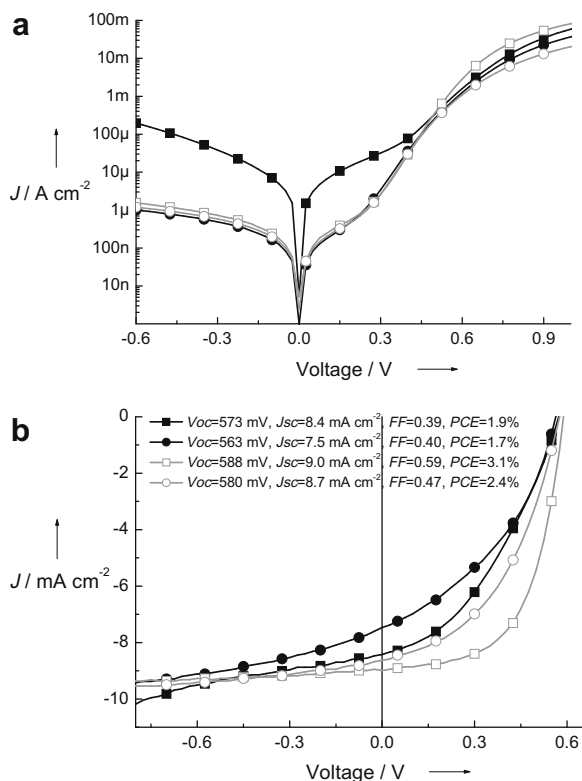


Fig. 3. Current density–voltage (J – V) characteristics of the devices under study: chlorobenzene (**IF1**) monolayer (black squares), chlorobenzene (**IF1**) bilayer (black dots), oDCB/mesitylene (**IF2**) monolayer (grey open squares) and oDCB/mesitylene (**IF2**) bilayer (grey open dots). (a) Representative dark J – V characteristics in a semi-logarithmic representation in the voltage range revealing the opening of the diode. (b) J – V curves under AM 1.5 illumination with 100 mW cm^{-2} .

The above equation represents the J – V characteristics of a solar cell according to a standard replacement circuit as demonstrated elsewhere [10], where J reveals the measured current density throughout the device, J_0 shows the reverse current of the diode (saturation current), V the applied voltage, R_s and R_p the serial and parallel resistances, J_{light} the photogenerated current of the device, e evidences the natural exponential function and q the elementary charge [10]. The diode ideality factor n represents the opening of the diode, which is the recombination at the interfaces between the donor and acceptor material. Therefore n correlates with the number of distributed interfaces within the blend [11] and reflects the morphology of the blend. The dark J – V curves (Fig. 3a) between 0 and the built in potential V_{BI} are characteristic for the diode behaviour of the solar cells, as defined by the ideality factor n and saturation current J_0 . Variations in the absolute values of n are related to different morphologies, where $n = 1$ is representative for a bilayer system and $n = 2$ represents an intimate mixing of the donor with the acceptor throughout the bulk. Values larger than 2 indicate more complex carrier recombination mechanisms. From the dark J – V characteristics between 0.3 and 0.6 V (Fig. 3a) all fabricated devices reveal, within the accuracy of the

analysis method, similar values for n in the range of 1.6–1.9 which are typical values for polythiophene:PCBM blend devices. The dark J – V curve of **IF1** spray coated monolayer (Fig. 3a, black squares) solar cell exhibits a huge limitation in the shunt and can therefore not be simulated with this model. The **IF1** spray deposited bilayer (Fig. 3a, black dots) and the doctor bladed equivalent (not shown) indicate similar values within the certainty of the fit of $n = 1.8 \pm 0.1$ and 1.9 ± 0.05 , respectively. Comparing the dark J – V characteristics of **IF2** based spray deposited devices (Fig. 3a, grey curves) with their doctor bladed equivalent (Fig. S2a), the differences are also within the certainty of the fit, namely $n = 1.8 \pm 0.1$ for the mono- and bilayer and $n = 1.6 \pm 0.05$ for the doctor bladed (dark J – V curve of doctor bladed device, see Supplementary information, Fig. S2a). For both solvents we can not measure a significant difference in the ideality factor between a spray coated and doctor bladed devices. Typically such an observation is explained by a rather comparable distribution of the donor and acceptor interface throughout the bulk of the heterojunction. Even though the similar ideality factors are not a direct proof for identical nanomorphologies, our experience on several material systems showed good correlation between ideality factor and morphology [10,11]. In contrast, there is a significant variation in the charge carrier extraction between the various spray coated solar cells (Fig. 3b) and doctor bladed devices (Fig. S2b). That variation is correlated to differences in the mobility–lifetime product as clearly seen by the simulations. The low $\mu\tau$ -product goes hand-in-hand with the lower fill factors for spray coated devices as discussed in more detail below. The AFM images show clear distinctions in the topography (Fig. 2). Furthermore, the dark J – V characteristics distinguish significantly in the series resistance R_s (Fig. 3a). Independent of the ink formulation, the monolayers demonstrate a lower R_s than the spray coated bilayers due to the lower film thickness for the monolayers. In addition, the dark J – V characteristics exhibit low leakage currents for the **IF1** bilayer (Fig. 3a, black dots), the **IF2** monolayer (Fig. 3a, grey open squares) and **IF2** bilayer (Fig. 3a, grey open dots), whereas the dark J – V curve of the monolayer based on **IF1** (Fig. 3a, black squares) reveals an atypical shape, low currents in forward direction and high leakage current in reverse bias indicating decreased bottom contact selectivity. The diagram in Fig. 3b summarizes the J – V characteristics under AM 1.5 illumination with 100 mW cm^{-2} . A clear difference in the device performance is visible comparing **IF1** with **IF2** devices. The **IF1** monolayer device (Fig. 3b, black squares) exhibits a V_{oc} of 573 mV, a short circuit current density (J_{sc}) of 8.4 mA cm^{-2} , a FF of 0.39 resulting in 1.9% PCE. The bilayer device based on **IF1** (Fig. 3b, black dots) shows the lowest solar cell parameters with $V_{oc} = 563$ mV, $J_{sc} = 7.5\text{ mA cm}^{-2}$, FF of 0.40 and a PCE of 1.7%. The strong limitation in FF for **IF1** devices is attributed to a reduced extraction of the charge carriers. In contrast, the **IF2** spray deposited devices perform significantly better, with a V_{oc} of 588 mV, J_{sc} of 9.0 mA cm^{-2} , a high FF of 0.59 for the monolayer (Fig. 3b, grey squares). This corresponds to a power conversion efficiency of 3.1%. The bilayer based on **IF2** (Fig. 3b, grey dots) features similar performance,

$V_{oc} = 580$ mV, $J_{sc} = 8.7$ mA cm⁻², but shows the main limitation in *FF* with 0.47 corresponding to a PCE of 2.4%. Comparing the shape of the *J-V* characteristics under illumination, there is an obvious distinction in the curve progression. Clearly, bilayer devices have lower *FF* due to the larger R_s . Moreover, a difference due to the mobility-lifetime ($\mu\tau$) product can be seen. The photogenerated carriers are field driven [10], therefore a product of internal field and $\mu\tau$ smaller than the film thickness will lead to a loss in photocurrent. At larger external negative bias the field for the carriers is large enough to be completely extracted, which can be seen for all illuminated *J-V* curves showing the same photocurrent at bias around -0.6 V. The monolayer of **IF2** (Fig. 3b, grey squares) shows a nearly constant photocurrent for voltages < 0.2 V. The thicker bilayer devices of **IF2** (Fig. 3b, grey dots) are affected by a $\mu\tau$ limitation, and it needs reverse bias of -0.3 V to extract all photogenerated carriers. The monolayer of **IF1** (Fig. 3b, black squares) shows also a lower photocurrent at 0 V than at -0.3 V, while the bilayer (Fig. 3b, black dots) shows a complete extraction only at -0.6 V. Monolayer devices with a thickness of 250 nm are much weaker field dependent than thicker bilayer devices. In good agreement with earlier reports [5], the more slowly dried **IF2** films have a larger $\mu\tau$ -product, sufficient to extract all carriers under J_{sc} conditions.

Fig. 4a represents the *J-V* behaviour of a fully spray coated device, comprising a 60 nm spray deposited PEDOT:PSS layer on top of ITO and a subsequent spray deposited P3HT:PCBM based on **IF2** (monolayer with 250 nm P3HT:PCBM film thickness; these parameters resulted in the most efficient spray coated active layer device). The fully spray deposited solar cell exhibits a decent device performance (Fig. 4a), V_{oc} of 560 mV, J_{sc} of 9.1 mA cm⁻² and a *FF* of 0.52. This corresponds to a power conversion efficiency of 2.7% for a fully spray coated device. Comparing the **IF2** monolayer reference solar cell device (grey open squares in Fig. 3) with the “fully sprayed” device comprising a spray deposited PEDOT:PSS and a spray coated P3HT:PCBM (*J-V* behaviour is shown in Fig. 4a), a clear difference of the device performance is visible, which can be attributed to the spray deposited PEDOT:PSS. The fully sprayed solar cell (see Fig. 4a) indicates a 5% lower V_{oc} (560 mV) compared to the **IF2** monolayer device with doctor bladed PEDOT:PSS, grey squares in Fig. 3b (588 mV), whereas the J_{sc} is in the same range (9.0 mA/cm² for **IF2** monolayer and 9.1 mA/cm² for fully sprayed solar cell). Comparing the *FF* of both devices, there is a clear distinction between the **IF2** monolayer reference and the fully sprayed solar cell device, namely 0.59 and 0.52, respectively. This lower *FF* for the fully sprayed solar cell is attributed to the spray deposited PEDOT:PSS due to higher surface roughness (rms = 20.7 nm) and higher leakage current, while same low R_s . Fig. 4b shows the AFM image of the PEDOT:PSS film with rms roughness of 20.7 nm and Fig. 4c reveals a reference doctor bladed PEDOT:PSS film with rms roughness of 3.7 nm. A significantly larger droplet size is observed for PEDOT:PSS spray coated films compared to spray deposited P3HT:PCBM layers. This larger droplet size is attributed to the higher surface tension of the water based PEDOT:PSS solution compared to the

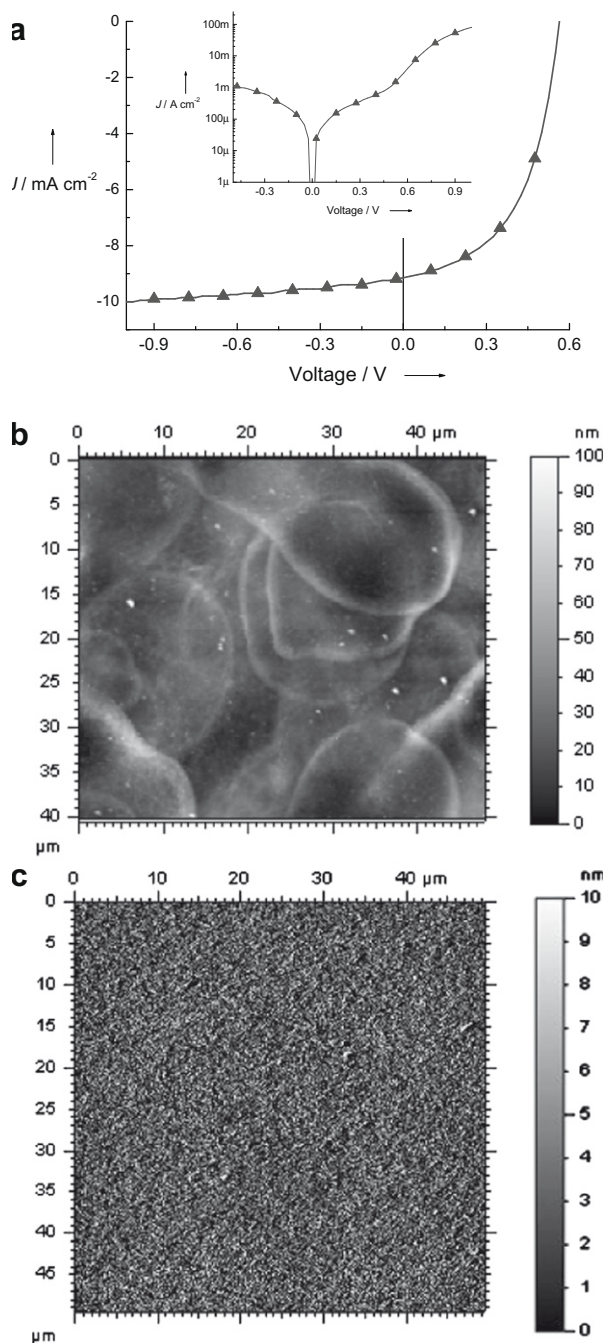


Fig. 4. Fully spray deposited solar cell with spray coated PEDOT:PSS and spray coated P3HT:PCBM. (a) *J-V* characteristics under AM 1.5 illumination with 100 mW cm⁻². The inset shows the dark *J-V* curve in a semi-logarithmic plot; (b) surface topography of a spray deposited PEDOT:PSS film and (c) surface topography of a reference doctor bladed PEDOT:PSS film.

P3HT:PCBM solution where smaller drop sizes can be created.

In this study, an alternative method is presented to deposit P3HT:PCBM blend and PEDOT:PSS to produce high efficiency devices. We discussed the topographical and

the nanomorphological aspects between a spray deposited mono- and bilayer based on a pristine solvent compared to a multiple solvent system. The AFM images in Fig. 2 indicate significant topographical differences between spray deposited and doctor bladed films. A J - V analysis (Fig. 3a) revealed similar ideality factors of mono- and bilayer spray coated films over doctor bladed ones indicating similar interface between the donor and acceptor in the BHJ, but differences in the charge carrier extraction between spray coated solar cells among themselves (Fig. 3b) and doctor bladed devices. The solvent properties such as boiling point, vapor pressure, viscosity and surface tension have a massive impact on the topography as shown by the AFM analysis. An optimized spray coating formulation is found with **IF2**, which allows to spray deposit films with outstanding high carrier transport properties, directly comparable to high qualitatively doctor bladed films. This resulted in an enhanced device performance with 3.1% PCE for spray coated polymer:fullerene based solar cells. Interestingly to note that the nearly 10 times higher surface roughness of **IF2** spray coated compared to doctor bladed films does not negatively influence the device performance. Moreover, we show that spray coating is a feasible technology to deposit among others also the PEDOT:PSS film without affecting the device parameters adversely. The high photovoltaic performance of 2.7% PCE for fully sprayed cells proves the outstanding potential of spray coating as a novel manufacturing method for organic electronics.

1. Experimental section

The devices were built on transparent indium tin oxide (ITO) coated glass substrates, purchased from TFD. The glass was cleaned for 10 min in acetone and another 10 min in isopropyl alcohol using an ultrasonic bath and finally with an ozone treatment lasting 10 min. A thin 60 nm layer of poly(3,4-ethylene dioxythiophene) doped with polystyrene sulphonic acid (PEDOT:PSS) was deposited by doctor blading on top of the ITO bottom electrode. For our devices the Baytron PH, comprising a PEDOT:PSS ratio of 1:2.5 by weight, purchased from H.C. Starck was used. After the PEDOT:PSS doctor blading step, the samples were stored in inert atmosphere for at least 2 h. For spray deposited PEDOT:PSS layers, the Baytron PH dispersion was diluted with deionized water in a ratio of 1:3. The thickness of the spray deposited PEDOT:PSS film was measured to be 60 nm. In comparison to doctor bladed PEDOT:PSS, the spray deposited PEDOT:PSS on ITO was used as prepared for the spray deposition of the P3HT:PCBM. The photoactive layer consists of 1.5 wt% P3HT blended with fullerene PCBM in a 1:0.8 weight ratio and dissolved in pristine chlorobenzene or ortho-dichlorobenzene/mesitylene solvent mixture. The deposition of the active layer by spray coating was performed with an airbrush system in ambient surroundings with 3 bar pressure. For the fabrication of bilayers, no additional drying procedure among mono- and bilayer deposition was applied, despite the delay of 2 min needed by the setup between the two successive spray deposited films. On top of the active layer, an

additional Ca–Ag top electrode was deposited by physical vapor deposition to complete the bulk heterojunction solar cell. Prior to evaporation of the top electrode, all devices were subjected to a thermal treatment at 140 °C for 10 min. For efficiency evaluation the device area was defined by the overlap between the underlying ITO and the top electrode. Solar cells with an active area of typically 20 mm² were studied. The current density–voltage (J - V) characteristics were assessed with a source measurement unit SMU 2400 from Keithley under nitrogen atmosphere. For illumination a Steuernagel Solarsimulator was used providing an AM 1.5G spectra at 0.1 W cm⁻². AFM images of the thermally annealed spray coated films were recorded on glass substrates coated with a 60 nm PEDOT:PSS layer with a NanoSurf easyScan 2 operating under ambient conditions in contact mode. Measurements were performed using a pointprobe-plus silicon-SPM cantilever. Surface tensions and contact angles were measured with a Krüss easy drop tool. The kinematic viscosity of the two blend formulations was determined at room temperature with a micro Ubbelohde capillary viscosimeter from Schott.

Acknowledgement

We would like to acknowledge Professor Jürgen Parisi for valuable discussions.

Appendix A. Supplementary data

Supplementary data associated with this article can be found, in the online version, at [doi:10.1016/j.orgel.2009.02.010](https://doi.org/10.1016/j.orgel.2009.02.010).

References

- [1] C.J. Brabec, J.A. Hauch, P. Schilinsky, Christoph Waldauf, MRS Bulletin 30 (2005) 50.
- [2] P. Schilinsky, C. Waldauf, C.J. Brabec, Adv. Funct. Mater. 16 (2006) 1669.
- [3] S.E. Shaheen, R. Radspinner, N. Peyghambarian, G.E. Jabbour, Appl. Phys. Lett. 79 (2001) 2996.
- [4] C.N. Hoth, S.A. Choulis, P. Schilinsky, C.J. Brabec, Adv. Mater. 19 (2007) 3973.
- [5] (a) Y. Kim, S. Cook, S.M. Tuladhar, S.A. Choulis, J. Nelson, J.R. Durrant, D.D.C. Bradley, M. Giles, I. McCulloch, C.S. Ha, M. Ree, Nature Mater. 5 (2006) 197; (b) W. Ma, C. Yang, X. Gong, K. Lee, A.J. Heeger, Adv. Funct. Mater. 18 (2006) 572; (c) G. Li, V. Shrotriya, J. Huang, Y. Yao, T. Moriarty, K. Emery, Y. Yang, Nature Mater. 4 (2005) 864; (d) S. Curran, D.L. Carroll, Org. Lett. 7 (2005) 5749.
- [6] NREL Certificate Konarka, 5.24% under AM1.5 spectrum, November 2006.
- [7] (a) T. Ishikawa, M. Nakamura, K. Fujita, T. Tsutsui, Appl. Phys. Lett. 84 (2004) 2424; (b) X.L. Mo, T. Mizokuro, H. Mochizuki, N. Tanigaki, T. Hiraga, Jpn. J. Appl. Phys., Part 1 44 (2005) 656.
- [8] D. Vak, S. Kim, J. Jo, S. Oh, S. Na, J. Kim, D. Kim, Appl. Phys. Lett. 91 (2007) 081102.
- [9] R. Green, A. Morfa, A.J. Ferguson, N. Kopidakis, G. Rumbles, S.E. Shaheen, Appl. Phys. Lett. 92 (2008) 033301.
- [10] (a) C. Waldauf, P. Schilinsky, J.A. Hauch, C.J. Brabec, Thin Solid Films 451–452 (2004) 503–507; (b) P. Schilinsky, C. Waldauf, J.A. Hauch, C.J. Brabec, J. Appl. Phys. 95 (2004) 5.
- [11] C. Waldauf, M.C. Scharber, P. Schilinsky, J.A. Hauch, C.J. Brabec, J. Appl. Phys. 99 (2006) 04503.